Redox Chemistry of Actinide Ions in Wells−Dawson Heteropolyoxoanion Complexes

Ming-Hsi Chiang,[a] L. Soderholm,*[a] and Mark R. Antonio*[a]

Keywords: Actinides / Cyclic voltammetry / Polyoxometalates / Redox chemistry / Nernst analysis / Intermediate valence / Spectroelectrochemistry / XANES

The redox behavior has been characterized for several actinide (*An*) complexes with the monovacant Wells–Dawson anion, of the form $[An^{n+}(\alpha\text{-}2\text{-}P_2W_{17}O_{61})_2]^{n-20}$ (*An* = Th^{4+}, U^{4+}, Np^{4+}, Pu^{4+}, and Am^{3+}). Two complexes, with *An* = U^{4+} and Am^{3+}, show redox activity under oxidizing conditions, which is attributed to the actinide oxidation. Am^{3+} is oxidized to Am^{4+} with an $E_{1/2}$ = +1.21±0.01 V, and U^{4+} oxidizes to U^{5+} with a measured $E_{1/2}$ = +0.55±0.01 V vs. Ag/AgCl. Although the cyclic voltammetry (CV) data are consistent with a reversible redox couple, bulk oxidative electrolysis of $[U^{4+}(\alpha\text{-}2\text{-}P_2W_{17}O_{61})_2]^{16-}$ results in the decomposition of this complex to produce uranyl acetate and the free monovacant Wells–Dawson anion. In contrast, all of the CV data from the actinide coordination complexes differ from equivalent data obtained from the $[\alpha\text{-}2\text{-}P_2W_{17}O_{61}]^{10-}$ ligand itself. There are two complexed An^{4+} ions, Np and Pu, that undergo reduction over the same potential range as the ligands themselves. In situ X-ray spectroelectrochemistry is used to quantify the actinide response. The Np^{4+}/Np^{3+} redox behavior is a classically single ion process, with a formal potential of –0.84±0.01 V that was determined from a Nernst plot of X-ray absorption near-edge structure (XANES) data. The Pu^{4+}/Pu^{3+} formal reduction potential in the complex $[Pu(\alpha\text{-}2\text{-}P_2W_{17}O_{61})_2]^{n-}$ was determined to be –0.17±0.01 V using the same methodology. However, in this latter case, the slope of the Nernst plot indicates that 0.72±0.03 electrons are involved in the reduction. This is a significant deviation from the 1 electron expected for the Pu couple, and is discussed in terms of the concomitant reduction of the P–W–O framework of the Wells–Dawson anion.

Introduction

Polyoxometalates (POMs) are inorganic, anionic ligands with properties that have found application in such diverse areas as catalysis,[1,2] energy storage[3] and nuclear waste processing.[4−6] Unlike more familiar ligands (e.g., H_2O, NH_3, halides, carbonates, etc.), many POMs are electroactive,[7] particularly the heteropolyoxoanions of general composition $[X_aM_bO_c]^{d-}$ (X = Si, P, S; M = Mo, W). It is this intrinsic electrochemical functionality of POMs that accounts for their renowned behavior as reversible multielectron oxidants. They can accommodate substantial variation in their overall net charge without significant structural change or decomposition. The reduced species are known as heteropoly blues[7] because of their intense coloration, which arises from the delocalization of the added electrons in bands attributable to the metal oxide framework atoms (M = Mo^{6+}, W^{6+}).

The Wells−Dawson heteropolyanion $\alpha\text{-}[P_2W_{18}O_{62}]^{6-}$, shown in Figure 1, is an electroactive POM that accepts 1−6 electrons into its P−W−O framework upon reduction in aqueous media, while retaining its framework structure.[8−10] Selected $-WO^{4+}-$ units can be removed, from either the belt (α-1) or the cap (α-2) positions, to form an anion that acts as a ligand, which forms complexes with a variety of cations. Specific to our interests are complexes with 5f actinide ions, of the form $[An^{n+}(\alpha\text{-}2\text{-}P_2W_{17}O_{61})_2]^{n-20}$ (n = 3 and 4), which have been reported for Pu,[11] Am,[11−17] and Bk.[14] These actinide ions, together with U^{4+} and Np^{4+}, are known to be electroactive themselves.[18] The one-electron redox chemistry for the An^{4+}/An^{3+} aquo ions of U, Np, Pu, and Bk is generally

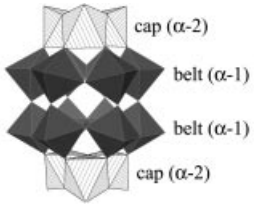

Figure 1. Polyhedral representation of the $\{W_{18}O_{62}\}$ framework of the plenary Wells−Dawson anion, $\alpha\text{-}[P_2W_{18}O_{62}]^{6-}$ showing the 6 capping W atoms (α-2 positions) as striped octahedra and the 12 belt W atoms (α-1 positions) as shaded octahedra; the two central $[PO_4]^{3-}$ tetrahedra are not shown

[a] Chemistry Division, Argonne National Laboratory,
9700 South Cass Avenue, Argonne, IL 60439-4831, USA
Fax: (internat.) + 1-630/252-4225
E-mail: ls@anl.gov, mantonio@anl.gov

facile and reversible, with tabulated standard electrode potentials in the range of $-0.773 \leq E^{\circ} \leq +1.47$ V vs. Ag/AgCl.[19]

In 1976, Saprykin et al.[11,20] reported that electroactive POMs, including the monovacant Wells–Dawson, exert a significant influence on the standard electrode potentials of the An^{4+}/An^{3+} redox couples. For example, in complexes of $[An^{4+}(\alpha\text{-}2\text{-}P_2W_{17}O_{61})_2]^{16-}$ (An^{4+} = Am, Cm, and Cf) the metal ions are stabilized toward reduction,[21] which would otherwise occur irreversibly on contact with water. From experimental measurements of the Wells–Dawson complexes of Pu^{4+},[11] Am^{3+},[11–17] and Bk^{3+},[14] the potentials for the An^{4+}/An^{3+} redox couple are approximately 1 V less than those tabulated for the standard reduction potentials, which correspond to the aquo ions in noncomplexing electrolytes.

Whereas it has been demonstrated that the substituted Wells–Dawson ligand can systematically shift the redox potential of bound 5f metal ions,[11–15,21] little work has been done to look for changes in the reduction response of the complexed anion. Of specific interest is the case, expected for the Np^{4+}/Np^{3+} and Pu^{4+}/Pu^{3+}couples, in which the reduction of the complexed *An* ion occurs over the same potential range as the reduction waves of the Wells–Dawson ligand itself. Under such conditions the localized f states are at the Fermi level of the P–W–O ligand states. Similar situations have been studied for f ions in transition-metal alloys, where correlated-electron and intermediate-valent phenomena have been observed.[22,23] Indeed, strong evidence of intermediate valence has been observed for Eu encrypted in the Preyssler anion, $[EuP_5W_{30}O_{110}]^{n-}$,[24] when the Eu f valence states are isoenergetic with the framework Fermi level. The systems under study herein provide a uniquely tunable and structurally simple model for extending studies of correlated electron behavior.

The objective of this study is to probe the electronic response of *An* Wells–Dawson complexes, in which both the f ion and the POM ligand are electroactive, to look for interactions that indicate f-state bonding or other unusual electronic responses. We report cyclic voltammetry and in situ XANES spectroelectrochemistry data on Th^{4+}, U^{4+}, Np^{4+}, and Pu^{4+} as well as Am^{3+}, some of which may give evidence of electronic interactions, but no strong evidence of intermediate valence is observed, even in cases where the P–W–O and f states are reduced concomitantly.

Results and Discussion

The CV data are shown in Figure 2 for the free ligand, $[\alpha\text{-}2\text{-}P_2W_{17}O_{61}]^{10-}$ (a, a′), and the cluster complexes, $[An^{n+}(\alpha\text{-}2\text{-}P_2W_{17}O_{61})_2]^{n-20}$ with Th^{4+} (b, b′), U^{4+} (c, c′), Np^{4+} (d, d′), Pu^{4+} (e, e′), and Am^{3+} (f, f′). These data were obtained under identical conditions, with the potential window limited by H_2 evolution at ≤ -1 V vs. Ag/AgCl and O_2 evolution at $\geq +1.4$ V vs. Ag/AgCl. The fundamental electrochemical parameters obtained from the data in Figure 2 are provided in Table 1 and compared in Table 2

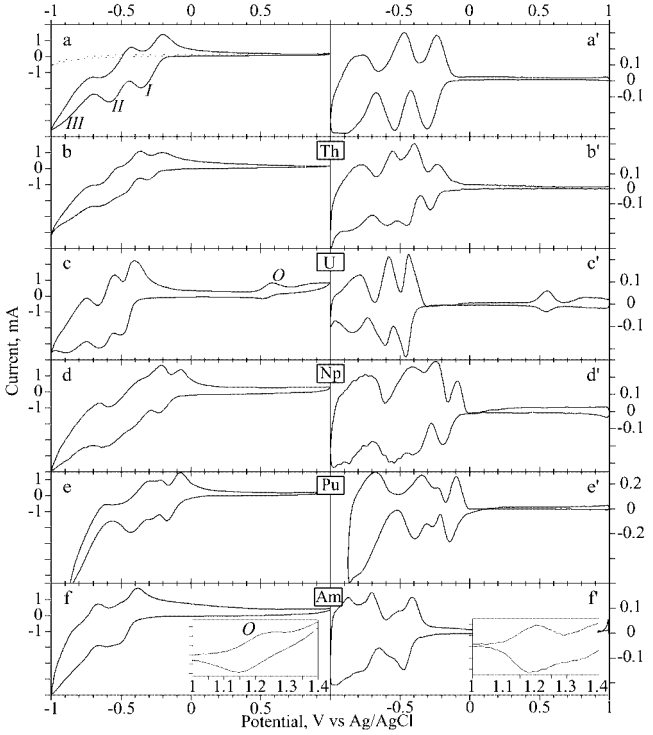

Figure 2. Left panels: cyclic voltammograms obtained at room temp. at 5 mV s^{-1} in supporting aqueous electrolytes (pH = 3.5) of 2:1 (v/v) mixtures of 0.5 M CH_3CO_2Li buffer at pH = 4.7 and 1 M $HClO_4$; right panels: the corresponding semi-differential data of the primary voltammograms; (a, a′) the uncomplexed ligand, $[\alpha\text{-}2\text{-}P_2W_{17}O_{61}]^{10-}$, including background scan (dashed line), revealing two well-resolved (*I*, *II*) redox waves and a third (*III*) less-resolved one; each arises from two-electron reduction processes of W^{6+} in the P–W–O band; by comparison, the complexes of Th^{4+} (b, b′), U^{4+} (c, c′), Np^{4+} (d, d′), Pu^{4+} (e, e′), and Am^{3+} (f, f′) with $[\alpha\text{-}2\text{-}P_2W_{17}O_{61}]^{10-}$ as $[An^{n+}(\alpha\text{-}2\text{-}P_2W_{17}O_{61})_2]^{n-20}$ cluster anions affect the reduction behavior of the ligand in significant fashion; all the solution species form heteropoly blues due to reduction of the P–W–O framework at potentials between 0 and −1 V; although the U^{4+} and Am^{3+} oxidation waves (labeled *O*) are visible in the CV data of (c, c′) and (f, f′), respectively, any evidence for the reduction of An^{4+} in $[An^{4+}(\alpha\text{-}2\text{-}P_2W_{17}O_{61})_2]^{16-}$ is not obvious because of the interfering response from the reduction of the ligand

with results from previous electrochemical investigations of $[An^{n+}(\alpha\text{-}2\text{-}P_2W_{17}O_{61})_2]^{n-20}$, as well as with the corresponding An^{n+} aquo ions.

The data in Figure 2 (a, a′) indicate that the free ligand has no electrochemical response under an oxidizing, positive, applied potential, consistent with the expectation that the W^{6+}–O valence band is empty. In contrast, the CV data for $[Am^{3+}(\alpha\text{-}2\text{-}P_2W_{17}O_{61})_2]^{17-}$, shown in Figure 2 (f, f′), exhibit an isolated redox wave under an oxidizing potential, at $E_{1/2} = +1.21 \pm 0.01$ V, that is attributed to the Am^{3+}/Am^{4+} couple. As evident from Table 2, our $E_{1/2}$ value is in agreement with previous polarographic and potentiometric measurements of the Am^{3+} oxidation potential in the $[Am^{3+}(\alpha\text{-}2\text{-}P_2W_{17}O_{61})_2]^{17-}$ complex measured in solutions with pH ranges of 2–5.[11,13–15] The measured reduction potential of +1.21 V is about 1.2 V less than the estimated standard electrode potential of +2.4 V for the Am^{4+} reduction in aqueous solution. This shift for the Am reduction potential upon complexation with the Wells–Dawson

Table 1. Electrode potentials [V vs. Ag/AgCl] of the redox couples obtained from the cyclic voltammetry data of Figure 2 for the free ligand, $[\alpha\text{-}2\text{-}P_2W_{17}O_{61}]^{10-}$, and the *An* complexes, $[An(\alpha\text{-}2\text{-}P_2W_{17}O_{61})_2]^{n-}$; the half-wave potentials, $E_{1/2}$, are presented as $(E_{pc} + E_{pa})/2$, where E_{pc} and E_{pa} are the cathodic and anodic peak potentials, respectively; the peak separations, ΔE_p, are presented as $E_{pa} - E_{pc}$, and "nr" means "not resolved"; errors associated with the values of E_{pc}, E_{pa}, $E_{1/2}$, and ΔE_p are either ±0.01 or ±0.005 V corresponding to the precision of the tabulated potentials

Anion	Wave	E_{pc} [V]	E_{pa} [V]	$E_{1/2}$ [V]	ΔE_p [V]
$[\alpha\text{-}2\text{-}P_2W_{17}O_{61}]^{10-}$	I	−0.357	−0.200	−0.28	0.157
	II	−0.584	−0.428	−0.51	0.156
	III	nr	−0.707		
$[Th(\alpha\text{-}2\text{-}P_2W_{17}O_{61})_2]^{16-}$	I	−0.308	−0.206	−0.26	0.102
	II	−0.48	−0.366	−0.42	0.114
	III	−0.64	−0.53	−0.59	0.110
	IV	nr	−0.70		
$[U(\alpha\text{-}2\text{-}P_2W_{17}O_{61})_2]^{16-}$	O	+0.516	+0.586	+0.55	0.070
	I	−0.504	−0.402	−0.45	0.102
	II	−0.648	−0.544	−0.60	0.104
	III	−0.886	−0.745	−0.82	0.141
$[Np(\alpha\text{-}2\text{-}P_2W_{17}O_{61})_2]^{16-}$	I	−0.230	−0.072	−0.15	0.158
	II	−0.448	−0.212	−0.33	0.236
	III	−0.619	−0.361	−0.49	0.258
	IV	nr	−0.652		
$[Pu(\alpha\text{-}2\text{-}P_2W_{17}O_{61})_2]^{16-}$	I	−0.172	−0.073	−0.12	0.099
	II	−0.298	−0.213	−0.26	0.085
	III	−0.431	−0.295	−0.36	0.136
	IV	nr	−0.605		
$[Am(\alpha\text{-}2\text{-}P_2W_{17}O_{61})_2]^{17-}$	O	+1.15	+1.26	+1.21	0.11
	I	−0.50	−0.382	−0.44	0.118
	II	−0.61	−0.50	−0.56	0.11
	III	nr	−0.67		
	IV	nr	−0.85		

Table 2. Standard electrode potentials [V vs. Ag/AgCl] for the *An* aquo ions in acid solutions at room temp. from the compilation of Bratsch;[19] the original values of Bratsch[19] in V vs. SHE were converted here to V vs. Ag/AgCl with respect to the redox potential (+0.196 V vs. SHE) for the BAS Inc. Ag/AgCl reference electrode (3 M NaCl) at 25 °C;[45] estimated values for which there are no experimental data are enclosed in parentheses; "na" = "not accessible" in aqueous electrolytes; "uk" = "unknown" in aqueous electrolytes; the sources of the potentials for the *An* Wells−Dawson complexes, $[An(\alpha\text{-}2\text{-}P_2W_{17}O_{61})_2]^{n-}$, in aqueous electrolytes at room temp. are given in the footnotes

An couple	Aquo ions 4+/3+	Wells−Dawson complexes 4+/3+	Wells−Dawson complexes 5+/4+
Th	na	na	na
U	−0.773	(−1.73)[a]	+0.56±0.01[b]
			+0.55±0.01[c]
Np	−0.039	(−0.95)[d]	uk
		−0.84±0.01[e]	
Pu	+0.810	−0.12±0.01[f]	uk
		−0.17±0.01[e]	
Am	(+2.4)	+1.20−1.26[g]	uk
		+1.21±0.01[c]	
		+1.33−1.39[h]	
		+1.05−1.10[i]	
Cm	(+2.8)	(+1.9±0.2)[j]	na
Bk	+1.47	+0.44[j]	na
Cf	(+3.1)	(+2.0±0.2)[j]	na

[a] From Erine et al.[37] [b] From Maslov et al.[27] [c] This work, $E_{1/2}$ value from cyclic voltammetry. [d] From Timofeev et al.[15] [e] This work, E°′ value from Nernst analysis of XANES spectroelectrochemical data. [f] From Saprykin et al.[11] [g] Range of values for 2≤pH≤5.[11,13−15] [h] Range of values for pH≤1.[12,17] [i] Range of values for pH ≈ 7.5 from Baranov et al.[16] [j] From Baranov et al.[14]

anion is somewhat larger than the −0.9 V that is typically seen for similarly complexed *An* ions.[11,15,21] Were it not for complexation with $[\alpha\text{-}2\text{-}P_2W_{17}O_{61}]^{10-}$, Am^{4+} would not be stable in aqueous solution. This stabilization of Am^{4+} by complexation with $[\alpha\text{-}2\text{-}P_2W_{17}O_{61}]^{10-}$ is the scientific basis for the separation process known as SESAME[5] and for aspects of the PARC process[6] in nuclear waste treatment operations.

$[U(\alpha\text{-}2\text{-}P_2W_{17}O_{61})_2]^{16-}$ also shows an electrochemical response under an oxidizing applied potential, with a redox wave [labeled *O* in Figure 2 (c, c′)] centered at $E_{1/2}$ = +0.55±0.01 V. Previous work has shown that, under the synthetic conditions employed in this study, U is tetravalent in $[U(\alpha\text{-}2\text{-}P_2W_{17}O_{61})_2]^{16-}$.[25] We argue that the redox wave observed here is due to the one-electron U^{4+}/U^{5+} couple. The one-electron oxidation of U^{4+} has been previously reported in both Keggin and Wells−Dawson heteropolyoxoanion complexes, $[U^{4+}(X^nW_{11}O_{39})_2]^{2n-20}$ ($X = Si^{4+}$; P^{5+}) and $[U^{4+}(P_2W_{17}O_{61})_2]^{16-}$.[26] The oxidation was achieved through electrolytic means, with electrode potentials of $+0.23 \le E^{\circ\prime} \le +0.64$ V, and through potentiometric titrations with dichromate and permanganate.[27] Our $E_{1/2}$ value agrees with the formal potential of +0.56±0.01 V obtained through a Nernst analysis of potentiometric data for $[U^{4+}(P_2W_{17}O_{61})_2]^{16-}$ by Maslov et al.[27]

A reliable standard potential for the one-electron oxidation of U^{4+}, unaccompanied by the formation of the linear dioxo moiety $[O{=}U^{5+}{=}O]^+$ is not available for comparison with our results. U^{5+} is unstable, so that, on contact with water, it invariably takes the form of the *trans*-dioxo cation $[UO_2]^+$, which itself is unstable with respect to disproportionation.[28] The observation of an apparently reversible voltammogram indicates that the coordination provided by the two Wells−Dawson ligands[25,29] provides a stabilizing environment for the dioxo-free (i.e., the so-called nude) U^{5+} cation.

In attempts to further characterize the U^{5+} complex of $[U(\alpha\text{-}2\text{-}P_2W_{17}O_{61})_2]^{15-}$, bulk electrolysis experiments were performed with the electrode polarized at +0.80 V. The solution color, which was initially violet, changed to red and then gradually faded to light pink as a white precipitate developed over the course of 1−18 h. Powder X-ray diffraction and EXAFS (extended X-ray absorption fine structure) data of the precipitate are consistent with a uranyl(VI) acetate phase.[30] On the longer time scale needed for bulk electrolysis, the U^{4+} oxidation is seen to be irreversible. On the significantly shorter time scale of cyclic voltammetry measurements, the U^{4+}/U^{5+} redox couple [*O* in Figure 2 (c, c′)] appears reversible, with a 0.070 V peak separation. This is likely to be a kinetic effect, in that the nude U^{5+} is sterically hindered, by the bulky Wells−Dawson ligands, from access

to the oxygen ligands necessary to form the dioxo moiety,

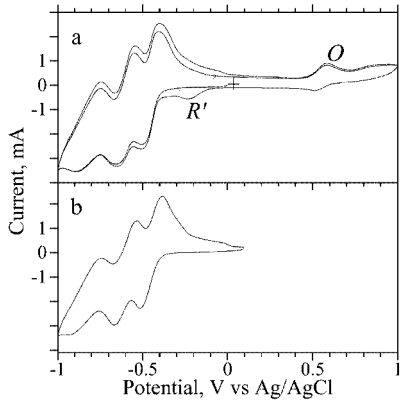

Figure 3. Cyclic voltammograms of $[U^{4+}(\alpha\text{-}2\text{-}P_2W_{17}O_{61})_2]^{16-}$; (a) starting from the initial potential of +0.1 V in a negative sweep to −1 V then to +1 V and back, showing the reversible U^{4+}/U^{5+} couple labeled *O* and the cathodic peak response labeled *R′* at −0.23 V attributed to reduction of $[UO_2]^{2+}$; (b) recorded 60 min after (a) starting from the initial potential of +0.1 V in a negative sweep to −1 V and back

$O{=}U^{5+}{=}O$. Yet, as shown in the CV data of Figure 3 (a), U demetalation is evident in successive sweeps with scan rates of 10 mV s^{-1} and slower between −1 and ≥ +0.6 V as the cathodic peak at −0.23 V labeled *R′*. This peak, which is otherwise not observed in shorter scans to ≤ +0.4 V as shown in Figure 3 (b), is the direct result of the redox couple *O* in Figure 3 (a). We suggest that peak *R′* is due to the reduction of $[UO_2]^{2+}$ (from cluster demetalation)[30] to U^{4+}, which subsequently combines with free ligand to reform the $[U^{4+}(\alpha\text{-}2\text{-}P_2W_{17}O_{61})_2]^{16-}$ complex. This would account for the absence of an anodic counterpart of *R′*, as would the irreversibility of the coupled electron transfer/chemical conversion between U^{4+} and $[UO_2]^{2+}$. No evidence is found for the reorganization of $[\alpha\text{-}2\text{-}P_2W_{17}O_{61}]^{10-}$, which can be readily reconstituted as $\alpha\text{-}[P_2W_{18}O_{62}]^{6-}$ and easily detected by CV.

In contrast to the sparse electrochemical responses of the actinide-coordinated, monovacant Wells−Dawson anions under oxidizing conditions, complicated redox responses are observed for all complexes under reducing conditions. The free ligand itself exhibits two well-resolved redox waves followed by one less-resolved wave, as indicated by *I*, *II*, and *III* in the voltammogram of Figure 2 (a). Previous work has attributed the waves to three 2-electron processes,[8,10,31−33] involving W^{6+} reduction. Extended Hückel calculations on the uncomplexed, plenary Wells−Dawson anion, $\alpha\text{-}[P_2W_{18}O_{62}]^{6-}$, indicate that the lowest unoccupied molecular orbital (LUMO) has a_1'' symmetry and is composed almost exclusively (96%) of metal orbitals derived from the 5d t_{2g} orbitals centered on the belt (α-1) tungsten atoms.[34] Symmetry requires that all 12 belt W atoms contribute with equal weight. The next higher energy state has e'' symmetry and is composed of both belt (61%) and cap (33%) positions.[34] Above these states in energy is another doubly degenerate set of orbitals that are located primarily (81%) on the cap positions, with only 12% on the belt positions.[34] The removal of a $W{=}O^{4+}$ moiety from the cap position, to form the α-2 derivative, lifts the threefold rotational symmetry of the parent ligand, and will lift the e states degeneracies. The first redox wave seen for $[\alpha\text{-}2\text{-}P_2W_{17}O_{61}]^{10-}$ in Figure 2 (a, a′) can thus be understood as arising from electron occupation in the LUMO that resides primarily on the belt (α-1) positions of Figure 1, and has a'' symmetry.[34−36]

Of the five *An* ions considered here, only Th^{4+} has no electroactivity of its own in the electrochemical region of interest. Yet, the complexation of electrochemically silent Th^{4+} modifies the voltammetric response of the P−W−O framework so that the $[Th(\alpha\text{-}2\text{-}P_2W_{17}O_{61})_2]^{16-}$ cluster has four redox waves. The first three are visible in the primary CV data of Figure 2 (b). The fourth one is less resolved but is seen clearly in the corresponding semiderivative data of Figure 2 (b′).

The reduction potentials of the An^{4+} ions coordinated by the monovacant Wells−Dawson anion are estimated by assuming a −0.9 to −1.0 V shift to the standard electrode potentials upon complexation.[15] Using this assumption, Np^{4+} and Pu^{4+} complexed with $[\alpha\text{-}2\text{-}P_2W_{17}O_{61}]^{10-}$ have reduction potentials that are expected to be accessible under our experimental conditions, whereas the estimated U^{4+}/U^{3+} potential of −1.73 V[37] is expected to be too low to be measurable. However, except for minor shifts in peak positions, the CV data for $[Np(\alpha\text{-}2\text{-}P_2W_{17}O_{61})_2]^{16-}$, shown in Figure 2 (d, d′), are essentially the same as those for $[Th(\alpha\text{-}2\text{-}P_2W_{17}O_{61})_2]^{16-}$ [Figure 2 (b, b′)], in which Th^{4+} has no redox activity. So, from the CV data alone, it is not possible to assign Np electrochemical activity to any specific feature that may otherwise arise from the redox activity of the P−W−O framework. Therefore, in order to evaluate the electrochemical response of these 5f ions under reducing conditions, optical spectroscopy and X-ray absorption experiments were undertaken.

Optical spectra were obtained for the yellow Np^{4+} solution complex and for the blue solution resulting from bulk electrolysis at −0.3 V vs. Ag/AgCl in order to assess the Np^{4+}/Np^{3+} redox activity in $[Np(\alpha\text{-}2\text{-}P_2W_{17}O_{61})_2]^{n-}$. These spectra are shown in Figure 4. The blue solution is optically dense and the electronic spectrum consists of weak bands attributable to the Np^{4+} complex superimposed on a strong and essentially featureless broad-band (460−1250 nm) ab-

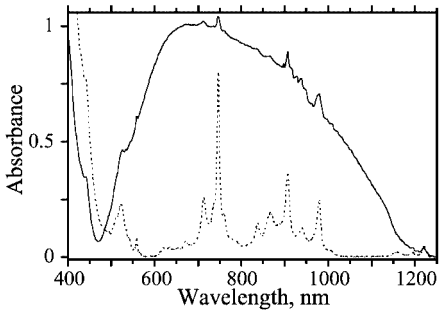

Figure 4. Optical spectrum of the transparent yellow solution of $[Np^{4+}(\alpha\text{-}2\text{-}P_2W_{17}O_{61})_2]^{16-}$ consistent with previous spectra[48−50] (dashed line) and the opaque heteropoly blue solution (solid line), following exhaustive electrolysis at −0.3 V

sorption associated with the reduction of the ligands. Absorption bands of similar breadth are found in the spectra for the heteropoly blues of $[\alpha\text{-}1\text{-}P_2W_{17}O_{61}]^{n-}$ [38] as well as $[PMo_{12}O_{40}]^{n-}$ in protic[39] and aprotic media.[40] In the heteropoly blues of $[Np(\alpha\text{-}2\text{-}P_2W_{17}O_{61})_2]^{n-}$ produced by bulk electrolysis at potentials more negative than −0.3 V, any evidence for absorption bands due to Np was obscured by the broad, intense absorption by the P−W−O anions. Because of this, we exploited element-specific in situ XANES spectroelectrochemistry[41] to quantify the Np^{4+}/Np^{3+} redox couple.

The Np L_3-edge XANES spectra for the valence-pure α_2 Wells−Dawson complexes of Np^{3+} and Np^{4+} are shown in Figure 5 as solid lines. These spectra are discussed in detail elsewhere.[25] The data collected at intermediate potentials, after exhaustive bulk electrolysis, are shown as dashed lines. The XANES spectra can be treated as linear combinations of the two end-member, valence-pure spectra,[41,42] thereby extracting the relative ratio of the oxidized to the reduced species for each potential. These data serve as input into the Nernst equation, $E = E^{\circ\prime} + RT\{\log([ox]/[red])\}/nF$, for which [ox] and [red] are the concentrations of the oxidized and reduced species, respectively; E is the applied potential, R is the gas constant, and F is Faraday's constant.

The number of electrons (n) involved in the Np redox reaction, as well as the formal electrode potential ($E^{\circ\prime}$) for the Np^{4+}/Np^{3+} couple are determined from the Nernst plot shown in Figure 6. The variation of applied potential with $\log([Np^{4+}]/[Np^{3+}])$ shown by the solid circles has a linear dependence. The best fit, with $R^2 = 0.988$, is shown as the solid line. The slope (RT/nF) of the fitted line is 0.061±0.003 V, corresponding to $n = 0.97\pm0.05$ electrons transferred at 25 °C, and the intercept is equal to $E^{\circ\prime} = -0.84\pm0.01$ V. The observation of a slope consistent with that expected for a 1-electron transfer indicates that the Np ion in the Wells−Dawson complex is acting as a well-behaved, single-ion redox couple. The measured Np^{4+} reduction potential of −0.84 V is similar to the value of −0.95 V estimated from published trends.[37]

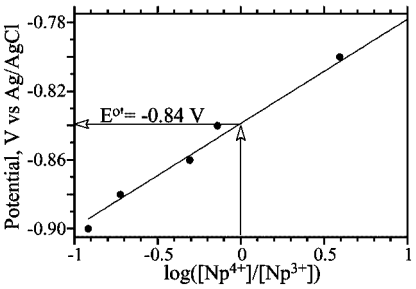

Figure 6. Nernst plot (circles) and best fit (line) with $R^2 = 0.988$ for $[Np(\alpha\text{-}2\text{-}P_2W_{17}O_{61})_2]^{n-}$; the slope, $RT/nF = 0.061\pm0.003$ V, provides the number of electrons (n) transferred in the Np^{4+}/Np^{3+} redox couple; at 25 °C, a slope of 0.05916 V corresponds to $n = 1$; we obtain $n = 0.97\pm0.05$; the X-axis intercept as indicated by the arrows provides the formal potential, $E^{\circ\prime} = -0.84\pm0.01$ V

The Pu^{4+} Wells−Dawson ion presents a situation similar to that of complexed Np^{4+} in that, under reducing conditions the CV data for $[Pu(\alpha\text{-}2\text{-}P_2W_{17}O_{61})_2]^{16-}$, shown in Figure 2 (e, e′), provide no obvious evidence for a Pu^{4+}/Pu^{3+} couple. This couple has been reported to have a formal potential of −0.12 V,[11] which is in the potential range for the observed P−W−O redox activity. Pu L_3-edge XANES experiments are used to quantify the Pu response, as a function of applied potential, from $[Pu(\alpha\text{-}2\text{-}P_2W_{17}O_{61})_2]^{n-}$. These data are shown in Figure 7. The concentrations, following bulk electrolysis, of Pu^{4+} and Pu^{3+} at each applied potential were used to construct the Nernst plot shown in Figure 8. The direct, linear dependence of potential vs. $\log([Pu^{4+}]/[Pu^{3+}]$ is evident in the primary data (solid circles) and by the best fit (solid line) with $R^2 = 0.998$. The formal potential, $E^{\circ\prime} = -0.17\pm0.01$ V, is determined from the intercept of this plot, and can be compared with that of -0.12 ± 0.01 V obtained by Saprykin et al.[11] This latter value was obtained by measurements of Eh in

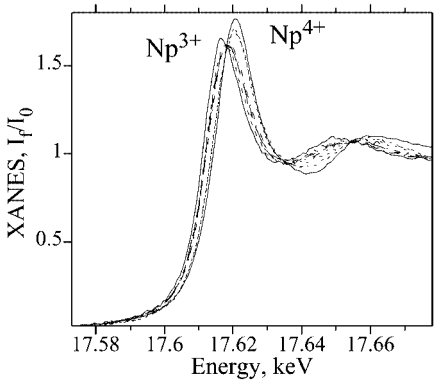

Figure 5. Normalized fluorescence XANES of the cluster anions containing valence-pure Np^{3+} and Np^{4+} (solid lines) obtained with the electrode polarized at −1.00 and +0.20 V, respectively, and with admixtures of both Np^{3+}- and Np^{4+}-containing anions (dashed lines) obtained with the electrode polarized at −0.900, −0.880, −0.860, −0.840, −0.800, and −0.780 V; as discussed elsewhere,[25] the L_3 XANES peaks for Np^{3+} and Np^{4+} are well resolved with a separation of 4.6 eV; this makes possible the quantitative analyses of the relative equilibrium concentrations of Np^{4+} and Np^{3+} in the admixtures[41]

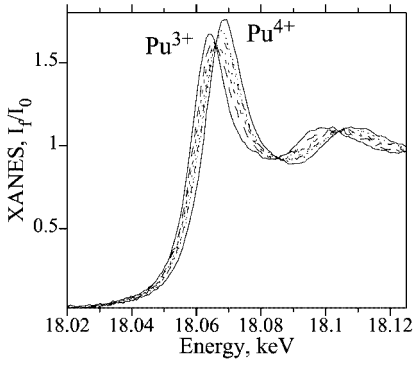

Figure 7. Normalized fluorescence XANES of the cluster anions containing valence-pure Pu^{3+} and Pu^{4+} (solid lines) obtained with the electrode polarized at −0.30 and +0.20 V, respectively, and with admixtures of both Pu^{3+}- and Pu^{4+}-containing species (dashed lines) obtained with the electrode polarized at −0.200, −0.180, −0.160, −0.140, and −0.120 V; as discussed elsewhere,[25] the L_3 XANES peaks for Pu^{3+} and Pu^{4+} are well resolved with a separation of 4.3 eV; this makes possible the quantitative analyses of the relative equilibrium concentrations of Pu^{4+} and Pu^{3+} in the admixtures[41]

non-blue solutions containing known mixtures of $[Pu^{4+/3+}(\alpha\text{-}2\text{-}P_2W_{17}O_{61})_2]^{16-/17-}$, prepared with preformed Pu^{4+} and Pu^{3+}. The slope (0.082 ± 0.003) of the Nernst plot of Figure 8 is 38% larger than expected for a one-electron Pu^{4+}/Pu^{3+} redox couple, and provides a smaller than expected value of $n = 0.72\pm0.03$ electrons transferred in the redox reaction. This value is significantly different from that expected for a well-behaved Nernstian system.[43]

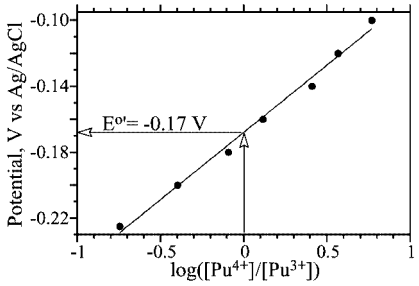

Figure 8. Nernst plot (circles) and best fit (line) with $R^2 = 0.998$ for $[Pu(\alpha\text{-}2\text{-}P_2W_{17}O_{61})_2]^{n-}$; the slope, $RT/nF = 0.082\pm0.003$ V, provides the number of electrons ($n = 0.72\pm0.03$) transferred in the Pu^{4+}/Pu^{3+} redox couple; the X-axis intercept as indicated by the arrows provides the formal potential, $E^{\circ\prime} = -0.17\pm0.01$ V

The high slope measured for the Pu^{4+} reduction may indicate weak interactions between the localized Pu f states and the P−W−O d-band states arising from correlated electron behavior. The redox couple, which has a formal potential of −0.17 V, is almost coincident with the first W-redox wave of the $[Pu(\alpha\text{-}2\text{-}P_2W_{17}O_{61})_2]^{16-}$ complex itself, which occurs at −0.12 V. This energy coincidence of localized f states with the W−O band states raises the possibility for correlated-electron behavior.[22,23] We have seen evidence for such f-P−W−O hybridization during the reduction of Eu^{3+} in the Preyssler POM, $[EuP_5W_{30}O_{110}]^{n-}$.[24] A Nernst plot, obtained from XANES data following a similar procedure to that used herein, is non-linear, with an applied potential range of 60 mV over which no change is observed in the $[Eu^{3+}]/[Eu^{2+}]$ ratio. Such behavior is consistent with that expected for a hybridization of the localized f_{Eu} states with the d_{W-O} band states because the added electrons are going into states comprised of both Eu and a large number of W. If the Pu f states and the d states on the 2 cap tungsten atoms had fully hybridized states, the electron would be shared between three centers, and the slope measured for the Pu reduction alone would be expected to be about 1/3. Therefore, an increased slope can be argued to be consistent with some degree of electron sharing among the cap-position ions. The linearity of the Pu Nernst response, as a function of applied potential, is consistent with the understanding that the W−O states that are reduced in the −0.12 V wave are those in the anion belt positions.[34−36] These states are expected to be electronically isolated from the cap-position states and therefore, although the criterion for intermediate-valent behavior is satisfied in terms of energetically isolated states in this experiment, the system symmetry prohibits the necessary spatial overlap of the appropriate wave functions.

The isolation of the first reduction wave, arising from the W atom in the belt positions, from the electronic states on the cap positions is further exemplified by the plot shown in Figure 9. The measured potentials of the W_{belt} redox waves are plotted as a function of An^{4+}−O bond length.[25] U^{4+} is not included in this plot because of the effects of the U^{5+}/U^{4+} couple (Figure 3) on cluster demetalation leading to the presence of free $[\alpha\text{-}2\text{-}P_2W_{17}O_{61}]^{10-}$ and $[UO_2]^{2+}$. The linear behavior ($R^2 = 0.999$) of this plot suggests dipolar interactions alone are primarily responsible for the slightly increased stability, of the W−O a′′ belt states, to reduction with increasing An−O bond length.

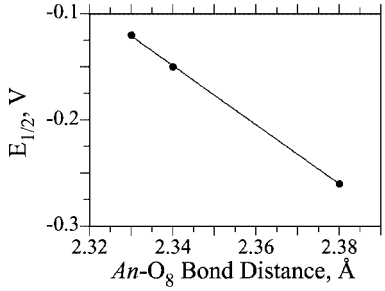

Figure 9. The decreasing half-wave, $E_{1/2}$, potentials of Table 1 for redox couple I (belt W reduction) of the Pu^{4+}, Np^{4+}, and Th^{4+} complex anions are plotted (circles) as a function of their increasing $An^{4+}-O_8$ bond lengths;[25] the best fit ($R^2 = 0.999$) is shown as a line with a slope of -2.79 ± 0.04 V/Å and an intercept of 6.37 ± 0.10 V

Conclusion

Although the reduction behaviors of both the actinide ion and the monovacant Wells−Dawson anion are altered upon their complexation, there is no evidence of significant hybridization between the An localized f states and the W−O band states. Specifically, the Pu^{4+}/Pu^{3+} redox couple is centered amongst the reduction waves of the anion itself. This situation may lead to intermediate valence[23] as has been demonstrated for $[EuP_5W_{30}O_{110}]^{n-}$ under similar conditions.[24] However, the Nernst plot obtained for Pu in $[Pu(\alpha\text{-}2\text{-}P_2W_{17}O_{61})_2]^{n-}$ is linear, although there appears to be an anomalously low number of electrons involved in the reduction. This result is interpreted in terms of electron delocalization into $Pu-W_{cap}$ states.

Experimental Section

CAUTION: Th, U, Np, Pu, and Am are radioactive elements. All experiments with these isotopes were performed in specialized laboratories using procedures designed and approved to minimize radiological and chemical hazards. For the transuranic elements, i.e., Np, Pu, and Am, their limited availability, together with radiation exposure concerns, require the use of only milligram quantities and thereby limit studies to small sample sizes. The $[An^{n+}(\alpha\text{-}2\text{-}P_2W_{17}O_{61})_2]^{n-20}$ complexes with natural Th^{4+} and U^{4+}, $^{237}Np^{4+}$, $^{242}Pu^{4+}$, and $^{243}Am^{3+}$ were prepared as described elsewhere.[25] Aqueous electrolytes of pH = 3.5, prepared from 2:1 (v/v) mixtures of 0.5 M CH_3CO_2Li buffer (pH = 4.7) and 1 M $HClO_4$, were used

for all measurements, which included optical, in situ Np and Pu XANES spectroelectrochemistry, and cyclic voltammetry (CV). Vis/NIR data were obtained with a Cary-14 Olis-conversion spectrometer. The in situ XANES was obtained with a purpose-built cell for spectroelectrochemistry.[41,44] CV data for the dilute (ca. 1 mM) solutions of $[An^{n+}(\alpha\text{-}2\text{-}P_2W_{17}O_{61})_2]^{n-20}$ were obtained under static conditions with scan rates of 5 mV s^{-1} in a single-compartment cell. The primary voltammograms were convolved by a semi-derivative method to provide clear visual resolution of the redox waves. All electrochemical operations (bulk electrolyses and CV) were performed with a BAS 100B/W electrochemical workstation and 6.15 mm diameter graphite rod (Alfa 14739) working and auxiliary electrodes, and a BAS (RE-5B) Ag/AgCl reference electrode (3 M NaCl). Unless specified otherwise, all measured and reported potentials are with reference to this electrode, with a redox potential of +0.196 V vs. SHE at 25 °C.[45] The background voltammogram of the neat electrolyte and clean electrodes was smooth and featureless over the range of potentials from −1 to +1.4 V. Np and Pu XANES spectra were recorded at the 7 GeV APS BESSRC CAT station 12-BM-B[46] as described previously.[25] With the dilute solutions of $[Np^{4+}(\alpha\text{-}2\text{-}P_2W_{17}O_{61})_2]^{16-}$ and $[Pu^{4+}(\alpha\text{-}2\text{-}P_2W_{17}O_{61})_2]^{16-}$ in the X-ray beam under vigorous sparging with N_2, we first collected data for the fully oxidized clusters at rest potential. This was followed by exhaustive (≥ 98%) electrolysis at −1.00 V and −0.30 V to produce the reduced heteropoly blue species with valence-pure Np^{3+} and Pu^{3+}, respectively, and XANES data acquisition. Thereafter, we recorded XANES data throughout the course of the stepwise oxidation by bulk electrolyses as a function of controlled potentials with the electrode polarized at −0.900, −0.880, −0.860, −0.840, −0.800, and −0.780 V for the Np complex, and at −0.225, −0.200, −0.180, −0.160, −0.140, −0.120, and −0.100 V for the Pu complex. X-ray and electrochemical spectra, obtained from the full re-oxidation of the reduced, Wells−Dawson complex, were indistinguishable from those obtained from the starting materials. This result confirms the reversibility of the redox chemistry. The Np and Pu XANES spectra obtained at the intermediate potentials were fit in a linear combination regression analysis with the pure An^{3+} and An^{4+} spectra using procedures in WinXAS[47] that have been described in detail elsewhere.[41,42] The relative partial concentrations for An^{4+} and An^{3+} obtained therewith were used for the Nernst plots of potential vs. $\log[Np^{4+}]/[Np^{3+}]$ and $\log[Pu^{4+}]/[Pu^{3+}]$.

Acknowledgments

We thank Clayton Williams and S. Skanthakumar of the Chemistry Division Actinide Facility as well as the staff of the BESSRC CAT at the Advanced Photon Source for assistance. This work is supported by the U.S. DOE, BES−Chemical Sciences and Material Sciences and, during the initial stages, by sponsorship of the Environmental Management Science Program, Office of Science and Technology, Office of Environmental Management, all under contract No. W-31-109-ENG-38.

[1] I. A. Weinstock, *Chem. Rev.* **1998**, *98*, 113−170.
[2] M. Sadakane, E. Steckhan, *Chem. Rev. (Washington, D.C.)* **1998**, *98*, 219−237.
[3] D. E. Katsoulis, *Chem. Rev.* **1998**, *98*, 359−388.
[4] L. Bion, P. Moisy, C. Madic, *Radiochim. Acta* **1995**, *69*, 251−257.
[5] C. Madic, J. Bourges, J.-F. Dozol, *AIP Conf. Proc.* **1995**, *346*, 628−638.
[6] M. Kamoshida, T. Fukasawa, F. Kawamura, *J. Nucl. Sci. Technol.* **1998**, *35*, 185−189.
[7] M. T. Pope, in *Mixed-Valence Compounds. Theory and Applications in Chemistry, Physics, Geology, and Biology* (Ed.: D. B. Brown), D. Reidel, Dordrecht, **1980**, pp. 365−386.
[8] R. Contant, J. P. Ciabrini, *J. Chem. Res. (S)* **1977**, 222.
[9] B. Keita, L. Nadjo, *J. Electroanal. Chem.* **1987**, *227*, 77−98.
[10] B. Keita, Y. W. Lu, L. Nadjo, R. Contant, *Eur. J. Inorg. Chem.* **2000**, 2463−2471.
[11] A. S. Saprykin, V. I. Spitsyn, N. N. Krot, *Doklady Phys. Chem. Engl. Transl.* **1976**, *228*, 500−502.
[12] V. N. Kosyakov, G. A. Timofeev, E. A. Erin, V. I. Andreev, V. V. Kopytov, G. A. Simakin, *Soviet Radiochem., Engl. Transl.* **1977**, *19*, 418−423.
[13] Y. M. Kulyako, I. A. Lebedev, V. Y. Frenkel, T. I. Trofimov, V. F. Myasoedov, *Soviet Radiochem., Engl. Transl.* **1981**, *23*, 674−679.
[14] A. A. Baranov, G. A. Simakin, V. N. Kosyakov, E. A. Erin, V. V. Kopytov, G. A. Timofeev, A. G. Rykov, *Soviet Radiochem., Engl. Transl.* **1981**, *23*, 104−106.
[15] G. A. Timofeev, V. M. Chistyakov, E. A. Erin, A. A. Baranov, V. V. Kopytov, *Soviet Radiochem., Engl. Transl.* **1986**, *28*, 156−161.
[16] A. A. Baranov, A. Y. Volkov, E. A. Erin, G. A. Timofeev, V. M. Chistyakov, *Radiochem., Engl. Transl.* **1996**, *38*, 474−476.
[17] D. Chartier, L. Donnet, J. M. Adnet, *Radiochim. Acta* **1999**, *85*, 25−31.
[18] L. R. Morss, in *Handbook on the Physics and Chemistry of Rare Earths*, vol. 18 (Eds.: K. A. Gschneidner, Jr., L. Eyring, G. R. Choppin, G. H. Lander), Elsevier Science, Amsterdam, **1994**, pp. 239−291.
[19] S. G. Bratsch, *J. Phys. Chem. Ref. Data* **1989**, *18*, 1−21.
[20] A. S. Saprykin, V. P. Shilov, V. I. Spitsyn, N. N. Krot, *Doklady Chem. Engl. Transl.* **1976**, *226*, 114−116.
[21] A. B. Yusov, V. P. Shilov, *Radiochem., Engl. Transl.* **1999**, *41*, 1−23.
[22] For example, see issue 48 (25 November 1996) of *J. Phys. Condens. Matter* **1996**, *8*.
[23] P. Fulde, *Electron Correlations in Molecules and Solids*, 3rd ed., Springer, Berlin, Germany, **1995**.
[24] L. Soderholm, M. R. Antonio, S. Skanthakumar, C. W. Williams, *J. Am. Chem. Soc.* **2002**, *124*, 7290−7291.
[25] M.-H. Chiang, C. W. Williams, L. Soderholm, M. R. Antonio, *Eur. J. Inorg. Chem.*, in press.
[26] S. C. Termes, M. T. Pope, *Trans. Met. Chem.* **1978**, *3*, 103−108.
[27] L. P. Maslov, L. V. Sirotinkina, A. G. Rykov, *Soviet Radiochem., Engl. Transl.* **1985**, *27*, 679−683.
[28] S. P. Best, R. J. H. Clark, R. P. Cooney, *Inorg. Chim. Acta* **1988**, *145*, 141−147.
[29] L. Bion, P. Moisy, F. Vaufrey, S. Meot-Reymond, E. Simoni, C. Madic, *Radiochim. Acta* **1997**, *78*, 73−82.
[30] Under the aqueous conditions used here, we suggest that the U^{5+} complex succumbs to hydrolytic attack liberating U^{5+}, which is rapidly oxidized to $[UO_2]^{2+}$.
[31] S. Dong, M. Liu, *J. Electroanal. Chem.* **1994**, *372*, 95−100.
[32] B. Keita, E. Abdeljalil, L. Nadjo, B. Avisse, R. Contant, J. Canny, M. Richet, *Electrochem. Commun.* **2000**, *2*, 145−149.
[33] B. Keita, F. Girard, L. Nadjo, R. Contant, J. Canny, M. Richet, *J. Electroanal. Chem.* **1999**, *478*, 76−82.
[34] B. Keita, Y. Jean, B. Levy, L. Nadjo, R. Contant, *New J. Chem.* **2002**, *26*, 1314−1319.
[35] X. Lopez, C. Bo, J. M. Poblet, *J. Am. Chem. Soc.* **2002**, *124*, 12574−12582.
[36] X. Lopez, C. Bo, J. M. Poblet, *Inorg. Chem.* **2003**, *42*, 2634−2638.
[37] E. A. Erine, A. A. Baranov, V. A. Yu, V. M. Chistyakov, G. A. Timofeev, *J. Alloys Compd.* **1998**, *271−273*, 782−785.
[38] B. Keita, A. Belhouari, L. Nadjo, R. Contant, *J. Electroanal. Chem.* **1998**, *442*, 49−57.
[39] P. Gómez-Romero, *Solid State Ionics* **1997**, *101−103*, 243−248.
[40] H. R. Sun, S. Y. Zhang, J. Q. Xu, G. Y. Yang, T. S. Shi, *J. Electroanal. Chem.* **1998**, *455*, 57−68.

[41] L. Soderholm, M. R. Antonio, C. Williams, S. R. Wasserman, *Anal. Chem.* **1999**, *71*, 4622−4628.
[42] M. R. Antonio, C. W. Williams, L. Soderholm, *Radiochim. Acta* **2002**, *90*, 851−856.
[43] J. O. M. Bockris, A. K. N. Reddy, *Modern Electrochemistry*, vol. 2, Plenum, New York, **1970**.
[44] M. R. Antonio, L. Soderholm, I. Song, *J. Appl. Electrochem.* **1997**, *27*, 784−792.
[45] A. W. Bott, *Curr. Sep.* **1995**, *14*, 64−68.
[46] M. A. Beno, M. Engbretson, G. Jennings, G. S. Knapp, J. Linton, C. Kurtz, U. Rütt, P. A. Montano, *Nucl. Instrum. Methods Phys. Res. A* **2001**, *467−468*, 699−702.
[47] T. Ressler, *J. Synchrotron Radiat.* **1998**, *5*, 118−122.
[48] V. P. Shilov, T. N. Bukhtiyarova, O. P. Zhuravleva, N. N. Krot, *Soviet Radiochem., Engl. Transl.* **1979**, *21*, 616−620.
[49] E. A. Erin, V. V. Kopytov, A. G. Rykov, V. Y. Vasil′ev, *Soviet Radiochem., Engl. Transl.* **1984**, *26*, 94−102.
[50] A. Y. Garnov, N. N. Krot, V. P. Perminov, *Radiochem., Engl. Transl.* **1998**, *40*, 7−10.

Received April 17, 2003

